DOI 10.1007/s11182-024-03151-y
Russian Physics Journal, Vol. 67, No. 5, May, 2024

PLASTIC DEFORMATION OF NANOCRYSTALLINE $Fe_{95}Ni_{05}$ WITH GRADIENT GRAINED STRUCTURE UNDER SHOCK LOADING

D. S. Kryzhevich, A. V. Korchuganov, A. S. Grigoriev, O. A. Berezikov, and K. P. Zolnikov

UDC 539.3:533.6.011.72

A molecular dynamics simulation of structural transformations in nanocrystalline $Fe_{95}Ni_{05}$ *samples with a single grain size and a gradient grained structure under shock loading is carried out. The shock loading condition is set by a constant-rate displacement of the non-deformable surface layer. It is found out that the generated shock wave is split into elastic and plastic components. An interaction of the plastic component with the grain boundaries leads to a generation of intrinsic stacking faults. The compressive stresses in the shock wave decrease as it propagates, which reduces the generation intensity of stacking faults and their density after stress relaxation. It is revealed that with a grain size increase, the density of the remaining stacking faults can significantly decrease, and the largest grains can completely restore the initial crystal structure after the shock wave propagation. By varying the grain structure, one can control the evolution of shock waves and the density of structural defects remaining in the material.*

Keywords: nanocrystalline structure, gradient nanograined structure, shock wave, plasticity, stacking fault, molecular dynamics

INTRODUCTION

The study of structural transformations in metallic materials under shock-wave loading is of significant interest for understanding the peculiarities of the changes in their physical and mechanical properties. The structural transformations in iron-based alloys under extreme conditions are of particular importance due to their widespread use in many industrial applications, geology and astrophysics. It is known that at high compression rates, the shock waves can split into elastic and plastic components [1]. With a further increase in the compression rate, one overdrive wave may appear [2]. In the materials undergoing phase transitions, the shock wave can have a three-wave structure, consisting of an elastic wave, a plastic wave, and a phase-transformed wave [3, 4]. The iron-based alloys are prototypical materials for studying such structural transformations under shock wave loading [5–7]. The formation of a three-wave structure in laser-shocked polycrystalline iron was confirmed by high-quality X-ray diffraction data [8]. An important property of a material having a significant impact on the response under shock loading is its internal structure. The presence of extended interfaces and different inclusions leads to a significant dissipation of the shock wave energy, which can manifest itself in the generation of structural defects and in the development of fracture processes [9].

Molecular dynamics (MD) is an effective computer simulation method for a detailed study of the mechanisms of deformation and fracture during shock loading of a material. It allows accurately calculating the parameters of the shock wave as it propagates. Modern MD simulations are applied to fairly representative samples containing tens of millions of atoms, which provides an atomic-level understanding of the structural response of a material under loading.

Institute of Strength Physics and Materials Science of the Siberian Branch of the Russian Academy of Sciences, Tomsk, Russia, e-mail: kryzhev@ispms.ru; avkor@ispms.ru; grigoriev@ispms.ru; berezikov07@ispms.ru; kost@ispms.ru. Original article submitted February 29, 2024.

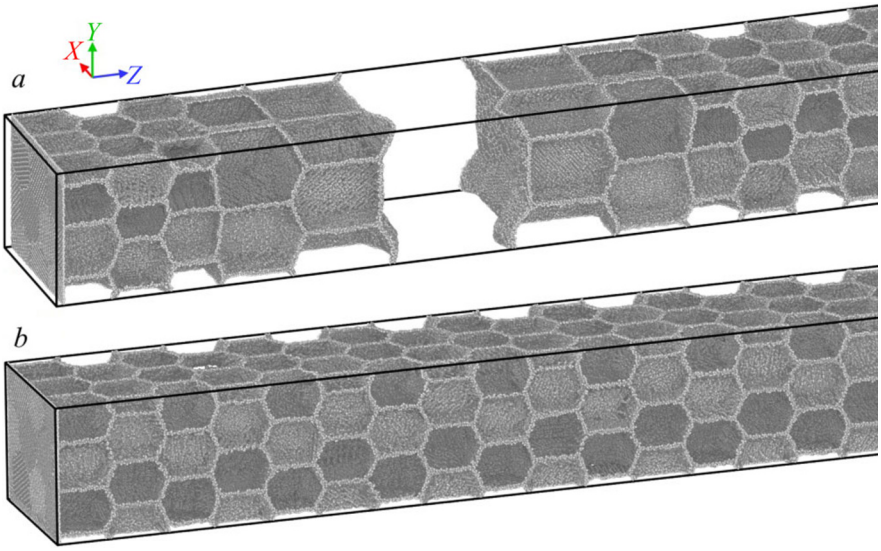

Fig. 1. Grain structure of the gradient nanograined (*a*) and 10 nm grain (*b*) samples. Image shows atoms in grain boundaries and on free surfaces only.

The behavior of complex structural materials, including nanocrystalline and energetic materials, under shock loading was reported in a large number of studies [10–18].

Gradient nanograined materials have unique physical and mechanical properties and are of significant interest for a wide range of practical applications. At the same time, the behavior of this class of materials under shock loading has not been sufficiently studied. In this study we perform an MD simulation of the behavior of a $Fe_{95}Ni_{05}$ nanocrystalline sample with a gradient grained structure and a nanocrystalline sample with one-size grains to identify the peculiarities of the plasticity nucleation and development in the material during the shock wave propagation.

MATERIALS AND METHODS

The behavior of nanocrystalline $Fe_{95}Ni_{05}$ samples under shock loading was studied via the calculations carried out using the LAMMPS software package [19]. The interatomic interaction in the Fe-Ni system was described by an embedded atom potential proposed by Zhou et al. [20]. To identify the structural changes in the loaded samples, the Common Neighbor Analysis algorithm was used [21].

The Voronoi–Laguerre method was applied for constructing a parallelepiped-shaped sample with a nanocrystalline gradient grained structure. All grains in the sample had a common crystallographic direction coinciding with the *Z* texture axis with indices [123] (Fig. 1). The simulated sample layers were successively arranged in the *Z* direction, starting from the free surface with the following grain sizes: 10, 10, 10, 15, 15, 30, 15, 15, and then 10 nm. A nanocrystalline sample with a grain size of 10 nm was also simulated under shock loading. Periodic boundary conditions were used along the *X* and *Y* directions, and free surfaces were simulated in the *Z* direction. The sample dimensions were 30×30×500 nm along the *X*, *Y* and *Z* directions, respectively. The initial temperature of the samples was 300°K.

To apply a shock loading, a non-deformable layer of a 5 Å thickness was set on the left side of the samples, which played the role of an impactor. It was displaced for 3 ps at a constant rate of 1.0 km/s and then defined as the deformable part of the sample with the free surface on the left side.

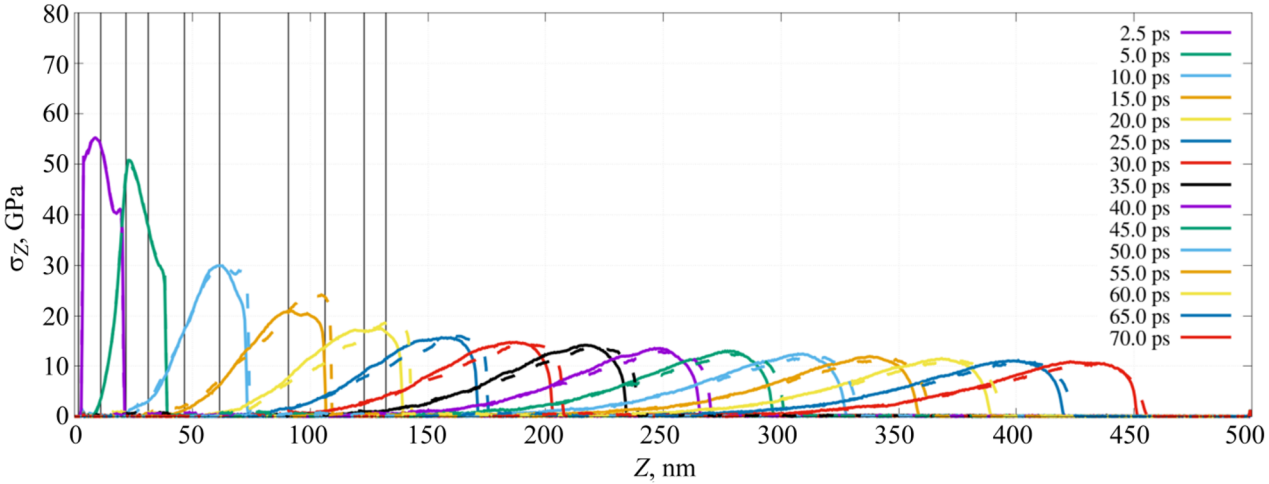

Fig. 2. Compressive stress distributions along the Z axis in the gradient nanograined sample (dashed lines) and the sample with 10 nm grains (solid lines) at different time instants. Vertical lines show the layer boundaries with different grain sizes in the gradient nanograined sample.

SIMULATION RESULTS

A comparison of the behavior of the nanocrystalline sample with 10 nm grains and that of the gradient nanograined sample under shock loading revealed the differences both in the shock wave propagation characteristics and in the defect structure formed in the samples. The position of the shock wave front and the shock wave length are clearly visible in the compressive stress distribution along the loading direction (Fig. 2). The maximum compressive stress in the shock waves decreases quite quickly and in 35–40 ps reaches saturation at ~12 GPa in both samples. The shock wave propagation front in the gradient nanograined sample accelerates and overrides that in the sample with 10 nm grains, as soon as the shock wave enters the layers with 15 nm grains. This is due to a weaker shock wave dissipation in the layers with larger grains, owing to a lower density of interfaces in these regions.

The grain structure differences in the samples lead to a different defect generation dynamics and a different defect structure formation after the end of relaxation processes. Intrinsic stacking faults are the main defects formed during shock impact, which persist after relaxation. To quantitatively compare the defect structures of the samples, we calculated the number of atoms composing stacking faults. The change in the spatial distribution of the atoms making up these defects for the simulated samples is shown in Fig. 3, wherein the local minima of the curves correspond to the sample regions with the maximum grain boundary density in the layers perpendicular to the Z axis. Figure 3 clearly shows that during the shock wave propagation, the number of atoms in the stacking faults changes quite strongly in the layers with different grain sizes. In each layer of grains, the stacking fault density quickly increases to a maximum value after the shock wave passage (its front is shown by the corresponding vertical dotted lines in Fig. 3). Then, as a result of accommodation processes, this density decreases more slowly due to the stacking fault closing by trailing partial dislocations sinking to the grain boundaries. Stacking faults are generated as a result of the shock wave interactions of s with the grain boundaries. This is clearly visible for the distribution of the stacking fault density at a time instant of 15 ps. Since the wave velocity is higher than that of partial dislocations forming the stacking faults, by this time instant the 30 nm grain (Z=60-90 nm) is filled with the stacking faults only in the left half. At the same time, the nucleation of stacking faults already begins at the boundary between this grain and the 15 nm grains (Z≈90 nm). Then these stacking faults propagate into both grain layers.

The stacking fault distribution in the sample along the loading direction stopped changing in 80 ps after the shock wave generation (Fig. 4). For the gradient nanograined sample, it is clearly seen that the layer with 30 nm grains

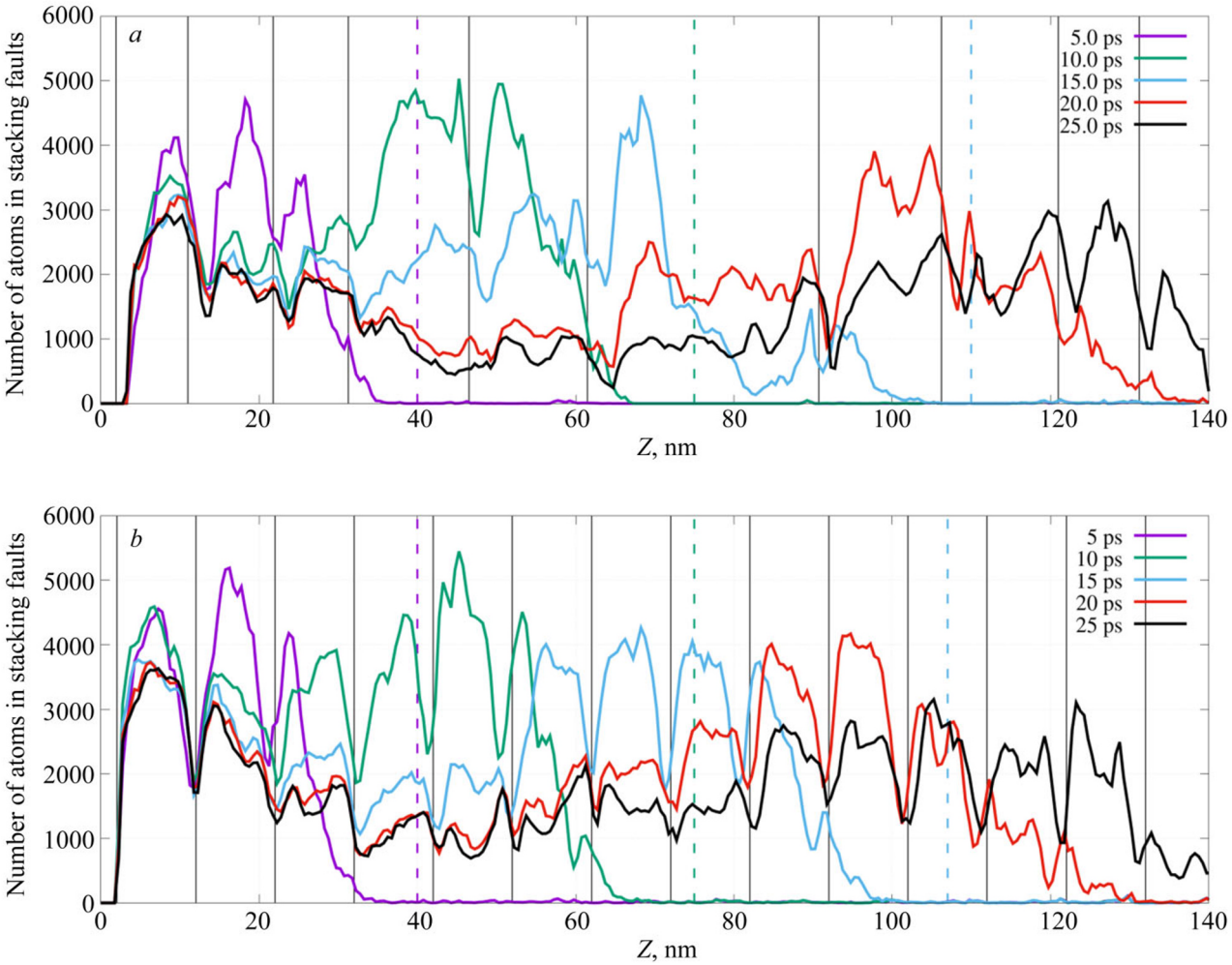

Fig. 3. Distributions along the Z axis of the number of atoms making up the stacking faults in the gradient nanograined sample (*a*) and in the sample with the 10 nm grains (*b*) at different time instants. Vertical lines show the layer boundaries with different grain sizes before loading. Positions of the shock wave front at different time instants are shown by dashed vertical lines.

contains virtually no stacking faults. On the left side of the sample (Z<60 nm), the stacking fault density is noticeably lower in the layer with 15 nm grains compared to 10 nm grains. In a sample with a single grain size of 10 nm, the density of the remaining stacking faults decreases in the shock wave propagation direction. This is due to a decrease in the compressive stresses in the shock wave during its propagation. Thus, a decrease in the compressive stresses in the shock wave and an increase in the grain size lead to a decrease in the density of the remaining stacking faults.

The simulations have shown that the shock wave splits into elastic and plastic waves. This splitting can be seen most clearly at the initial moments, when the compressive stresses have the highest values (Fig. 5). Figure 5 shows that for the given instant of time, the maximum coordinate Z=67 nm, at which stacking faults nucleate, corresponds to the plastic wave front. Note that the shock wave splitting into elastic and plastic components was observed in nanocrystalline iron samples [2, 22].

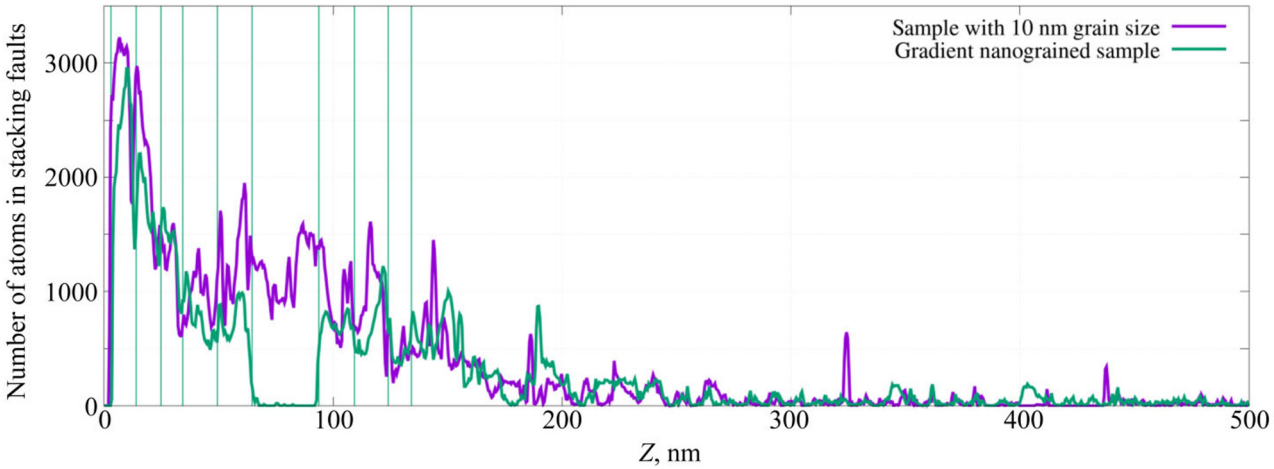

Fig. 4. Distributions along the *Z* axis of the number of atoms composing stacking faults in the gradient nanograined sample and the sample with the 10 nm grains 80 ps after shock loading. Vertical lines show the layer boundaries with different grain sizes in the gradient nanograined sample.

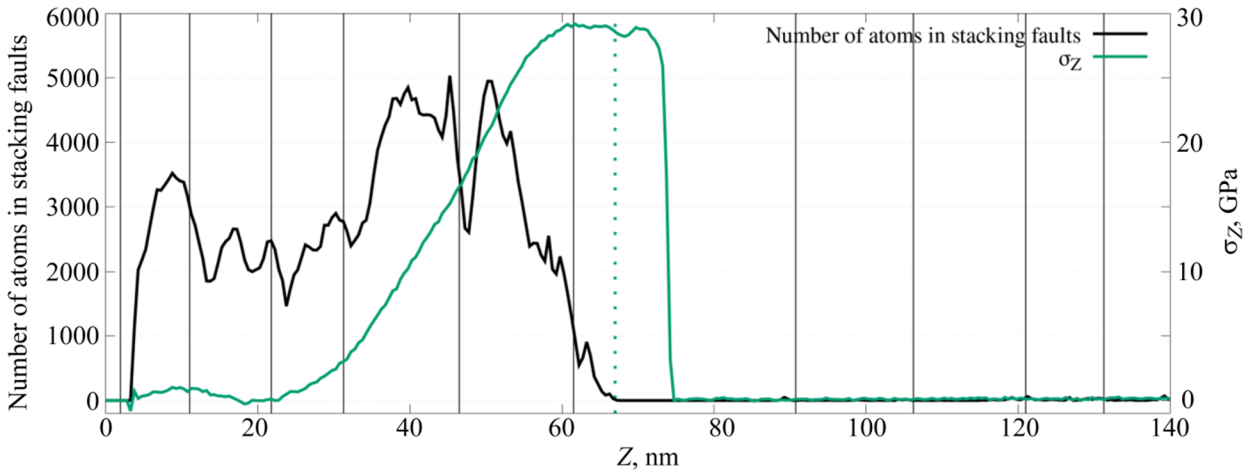

Fig. 5. Distribution of atoms composing stacking faults and compressive stresses along the *Z* axis 10 ps after shock wave initiation in the gradient nanograined sample. Vertical solid lines show the layer boundaries with different grain sizes before loading. Dotted line shows *Z* coordinate of plastic wave front.

CONCLUSIONS

Based on the simulations performed, we can conclude that the dynamics of structural transformations during shock wave propagation and the distribution of structural defects in the nanocrystalline sample with a single grain size and in the gradient nanograined sample are quite different. These differences are associated with the characteristics of the grain structure of the samples. It has been shown that the layers with larger grains in the gradient nanograined sample contain fewer stacking faults compared to that with smaller grains after the completion of the relaxation

processes. In the nanocrystalline sample with a single grain size, more stacking faults remain compared to the gradient nanograined sample under the same shock loading conditions. A decrease in the compressive stresses in the shock wave and an increase in the grain size lead to a decrease in the density of the remaining stacking faults. Thus, by creating a certain grain size gradient, it is possible to control the plastic deformation characteristics and the defect density in nanocrystalline materials with gradient grained structure under shock wave loading.

COMPLIANCE WITH ETHICAL STANDARDS

Author contributions

D.S.K.: conceptualization, writing of initial draft; A.V.K. and A.S.G.: development of the simulation approaches and performing the computations; O.A.B.: analysis and visualization; K.P.Z. verification of the results. All authors discussed the results and contributed to the final manuscript. All authors have read and agreed to the published version of the manuscript.

Conflicts of interest

The authors declare that they have no known competing financial interests or personal relationships that could have appeared to influence the work reported in this paper.

Funding

The study of a nanocrystalline sample with a single grain size was carried out according to the Government Assignment for the ISPMS SB RAS (Project No. FWRW-2021-0002). The study of the gradient nanograined sample was financially supported by the Russian Science Foundation (Project No. 20-79-10406), https://rscf.ru/project/20-79-10406/.

Financial interests

The authors have no relevant financial or non-financial interests to disclose.

Institutional review board statement

Applicable.

REFERENCES

1. M. A. Meyers, Dynamic behavior of materials (Wiley, 2007). https://doi.org/10.1002/9780470172278.
2. N. Gunkelmann, D. R. Tramontina, E. M. Bringa, and H. M. Urbassek, New J. Phys., **16**, 093032 (2014). https://doi.org/10.1088/1367-2630/16/9/093032.
3. J. C. Boettger and D. C. Wallace, Phys. Rev. B, **55**, 2840 (1997). https://doi.org/10.1103/PhysRevB.55.2840.
4. R. F. Smith, J. H. Eggert, R. E. Rudd, *et al.*, J. Appl. Phys., **110**, 123515 (2011). https://doi.org/10.1063/1.3670001.
5. B. J. Jensen, G. T. Gray, and R. S. Hixson, J. Appl. Phys., **105**, 103502 (2009). https://doi.org/10.1063/1.3110188.

6. J. A. Hawreliak, B. El-Dasher, H. Lorenzana, *et al.*, Phys. Rev., **83**, 144114 (2011). https://doi.org/10.1103/PhysRevB.83.144114.
7. R. F. Smith, J. H. Eggert, D. C. Swift, *et al.*, J. Appl. Phys., **114**, 123515 (2013). https://doi.org/10.1063/1.4839655.
8. H. Hwang, E. Galtier, H. Cynn, *et al.*, Sci. Adv., **6**, eaaz5132 (2020). https://doi.org/10.1126/sciadv.aaz5132.
9. I. A. Bryukhanov, Int. J. Plast. **151**, 103171 (2022). https://doi.org/10.1016/j.ijplas.2021.103171.
10. S. C. Hu, J. W. Huang, Z. D. Feng, *et al.*, J. Appl. Phys., **129**, 075902 (2021). https://doi.org/10.1063/5.0033153.
11. H. T. Luu, R. J. Ravelo, M. Rudolph, *et al.*, Phys. Rev. B, **102**, 020102 (2020). https://doi.org/10.1103/PhysRevB.102.020102.
12. P. G. Heighway, D. McGonegle, N. Park, *et al.*, Phys. Rev. Mater., **3**, 083602 (2019). https://doi.org/10.1103/PhysRevMaterials.3.083602.
13. L. Wang, B. Li, X. L. Deng, *et al.*, Phys. Rev. B, **99**, 174103 (2019). https://doi.org/10.1103/PhysRevB.99.174103.
14. D. R. Tramontina, E. N. Hahn, M. A. Meyers, and E. M. Bringa, AIP Conf. Proc., **1793**, 070002 (2017). https://doi.org/10.1063/1.4971590.
15. M. M. Sichani and D. E. Spearot, Comput. Mater. Sci., **108**, 226 (2015). https://doi.org/10.1016/j.commatsci.2015.07.021.
16. X. F. Wang, G. Tao, P. Wen, *et al.*, J. Phys. Chem. B, **124**, 9535 (2020). https://doi.org/10.1021/acs.jpcb.0c06077.
17. U. Adhikari, A. Goliaei, and M. L. Berkowitz, J. Phys. Chem. B, **119**, 6225 (2015). https://doi.org/10.1021/acs.jpcb.5b02218..
18. X. M. Lu, B. Yuan, X. R. Zhang, *et al.*, Appl. Phys. Lett., **110**, 023701 (2017). https://doi.org/10.1063/1.4973592..
19. S. Plimpton, J. Comput. Phys., **117**, 1 (1995). https://doi.org/10.1006/jcph.1995.1039.
20. X. W. Zhou, M. E. Foster, and R. B. Sills, J. Comput. Chem., **39**, 2420 (2018). https://doi.org/10.1002/jcc.25573.
21. J. D. Honeycutt and H. C. Andersen, J. Phys. Chem., **91**, 4950 (1987). https://doi.org/10.1021/j100303a014.
22. L. M. Barker and R. E. Hollenbach, J. Appl. Phys., **45**, 4872 (1974). https://doi.org/10.1063/1.1663148.